Published in final edited form as:
Biochemistry. 2013 October 29; 52(43): . doi:10.1021/bi4010864.

Splicing Kinase SRPK1 Conforms to the Landscape of Its SR Protein Substrate†

Brandon E. Aubol, **Michael Jamros**, **Maria L. McGlone**, and **Joseph A. Adams***
[1]Department of Pharmacology, University of California, San Diego, La Jolla, CA 92093-0636

[2]Department of Cellular & Molecular Medicine, University of California, San Diego, La Jolla, CA 92093-0636

Abstract

The splicing function of SR proteins is regulated by multisite phosphorylation of their C-terminal RS (arginine-serine rich) domains. SRPK1 has been shown to phosphorylate the prototype SR protein SRSF1 using a directional mechanism in which eleven serines flanked by arginines are sequentially feed from a docking groove in the large lobe of the kinase domain to the active site. While this process is expected to operate on lengthy arginine-serine repeats (≥8), many SR proteins contain smaller repeats of only 1–4 dipeptides raising the question of how alternate RS domain configurations are phosphorylated. To address this, we studied a splice variant of Tra2β that contains a C-terminal RS domain with short arginine-serine repeats [Tra2β(ΔN)]. We showed that SRPK1 selectively phosphorylates several serines near the C-terminus of the RS domain. SRPK1 uses a distributive mechanism for Tra2β(ΔN) where the rate-limiting step is dissociation of the protein substrate rather than nucleotide exchange as in the case of SRSF1. While a functioning docking groove is required for efficient SRSF1 phosphorylation, this conserved structural element is dispensable for Tra2β(ΔN) phosphorylation. These large shifts in mechanism are likely to account for the slower, net turnover rate of Tra2β(ΔN) compared to SRSF1 and may signal fundamental differences in phosphorylation among SR proteins with distinctive arginine-serine profiles. Overall, these data indicate that SRPK1 conforms to changes in RS domain architecture using a flexible kinetic mechanism and selective usage of a conserved docking groove.

The splicing of precursor mRNA (pre-mRNA) occurs in a macromolecular complex composed of several small nuclear RNAs and more than 100 auxiliary protein factors (1). This complex known as the spliceosome establishes the correct 5’-3’ splice sites and catalyzes the necessary transesterification reactions for splicing. Many proteins involved in this process contain polypeptide regions enriched in Arg-Ser dipeptide repeats known as RS domains. Most notably, the SR proteins are an essential family of splicing factors that derive their names from the presence of C-terminal RS domains. SR proteins typically bind to exonic sequences in pre-mRNA via their RNA recognition motifs (RRMs), recruiting essential elements of the spliceosome such as U1 snRNP at the 5’ splice site and U2AF65 at the 3’ splice site (2, 3). The activities of SR proteins are regulated through RS domain phosphorylation. The SRPK family of serine kinases phosphorylates SR proteins in the cytoplasm, a modification that initiates contacts with a transportin protein and directs the splicing factor into the nucleus (4, 5). SR proteins can undergo additional phosphorylation in the nucleus by SRPKs and the CLK family of protein kinases (6). There is now strong data supporting the notion that RS domain phosphorylation by these two kinase families not only controls the subcellular localization of SR proteins but also their role in gene splicing (7–

†This work was supported by NIH grants GM67969 and GM98528 to J.A.A.

*To whom correspondence should be sent: Joseph A. Adams, Tel: 858-822-3360; Fax: 858-822-3361; j2adams@ucsd.edu.

11). How SR protein phosphorylation controls splicing is not fully understood but recent progress suggests that the RS domain may regulate RRM interactions with pre-mRNA in a phosphorylation-dependent manner that requires the concerted activities of SRPKs and CLKs (12).

The RS domains in SR proteins can range from only 50 to over 300 residues in length and the Arg-Ser dipeptide repeats can vary in both length and position. To date, there is no universal understanding of how these domains are modified by SRPKs and CLKs and how specific phosphorylation regulates SR protein activities in splicing. Much of what we know about SR protein phosphorylation has been garnered from studies on the SR protein SRSF1 (aka ASF/SF2). SRSF1 is considered the prototype for the SR protein family and is the best understood, to date. It possesses two RRMs (RRM1 and RRM2) and a short RS domain (Fig. 1A). Prior kinetic studies showed that SRPK1 rapidly phosphorylates a long Arg-Ser stretch using a semi-processive, sequential mechanism in which the kinase binds with high affinity to the C-terminal end of the repeat and adds phosphates in a strict N-terminal direction (13, 14). This directional pathway is enforced by an electronegative docking groove in the large lobe of the kinase domain that systematically feeds N-terminal Arg-Ser dipeptides into the active site of SRPK1 (15). Translocation of the Arg-Ser dipeptides is highly efficient such that ADP release limits the addition of each phosphate (16, 17). Once this reaction is complete, SRPK1 can migrate to the C-terminal end of the RS domain and then slowly phosphorylate a shorter Arg-Ser stretch (3 repeats). CLK1 can modify the same serines as SRPK1 albeit at a slower rate. The kinase can also phosphorylate serines that flank prolines, an activity unique to the CLK family (18, 19). Unlike SRPK1 which moves in a highly directional manner, CLK1 appears to randomly phosphorylate the RS domain of SRSF1 (20). Despite these differences, both kinases bind SRSF1 with high affinity (K_d < 100 nM) (21).

While SRSF1 contains a lengthy Arg-Ser repeat region (Fig. 1A), many SR proteins contain smaller repeats of only 1–4 dipeptides that are unevenly and widely distributed in the RS domains (Fig. S1). Whether SRPK1 uses a common mechanism to modify these shorter repeats is not understood at this time. To investigate diverse modes of RS domain phosphorylation, we chose an alternative substrate that contains shorter Arg-Ser repeats in its C-terminal RS domain. Tra2β1 is an SR-like protein that contains two RS domains that flank the N- and C-terminal ends of a central RRM and is known to regulate the splicing of several genes including survival motor neuron 2 and Tau in a phosphorylation-dependent manner (22, 23). In addition to controlling pre-mRNA binding, RS domain phosphorylation blocks inclusion of exons 2 and 3 resulting in the expression of a truncated protein form of Tra2β1 [Tra2β3] that lacks the N-terminal RS domain and, thus, possesses the classic domain organization of an SR protein (24). This splicing switch has been correlated with the generation of Tau isoforms that could be linked to neurodegenerative diseases (25). The C-terminal RS domain of Tra2β3 differs from that of SRSF1 in that it lacks a lengthy Arg-Ser repeat and, thus, serves as a useful substrate for exploring the mechanism of SRPK1 toward alternate RS domains. We expressed and studied the phosphorylation of a form of Tra2β1 that lacks the N-terminal RS domain [Tra2β(ΔN)] mimicking the splice variant Tra2β3. We found that Tra2β(ΔN) is rapidly phosphorylated in the active site of SRPK1 but is turned over very slowly compared to the prototype SRSF1. This is due to a distributive phosphorylation mechanism in which protein translocation/release limits net turnover. These mechanistic changes account for the sluggish activation of Tra2β(ΔN) compared to SRSF1 and may reflect a general phenomenon for SR proteins with shorter Arg-Ser repeats. As a result of changes in the structure of the RS domain, the interaction of SRPK1 with Tra2β(ΔN) is profoundly different than that with SRSF1. Mutagenesis experiments show that a conserved docking groove in SRPK1, critical for rapid, directional phosphorylation of SRSF1, is dispensible for Tra2β(ΔN) phosphorylation. These results imply that splicing

kinases such as SRPK1 adapt to changes in the structural landscape of its substrate using unique mechanisms of catalysis tailored to the nature of the RS domain.

Materials & Methods

Materials

Adenosine triphosphate (ATP), 3-(*N*-morpholino)propanesulphonic acid (Mops), Tris (hydroxymethyl) aminomethane (Tris), $MgCl_2$, NaCl, EDTA, glycerol, sucrose, acetic acid, Lysozyme, DNAse, RNAse, Phenix imaging film, BSA, Whatman P81 grade filter paper, and liquid scintillant were obtained from Fisher Scientific. *Lysobacter enzymogenes* endoproteinase Lys-C (LysC) and protease inhibitor cocktail were obtained from Roche. [γ-^{32}P] ATP was obtained from NEN Products, a division of Perkin-Elmer Life Sciences.

Expression and Purification of Recombinant proteins

SRPK1, CLK1 and SRSF1 were expressed from a pET19b vector containing a 10xHis Tag at the N terminus (19). Tra2β(ΔN) which lacks resides 1–113 from Tra2β1 was expressed from pET28a containing a C-terminal 10XHis Tag. All mutations in Tra2β(ΔN) were generated by single or sequential polymerase chain reactions using the QuikChange™ mutagenesis kit and relevant primers (Stratagene, La Jolla, CA). All deletion constructs of Tra2β(MN) were generated using Thermo Scientific Phusion Site-Directed Mutagenesis Kit and relevant primers (Integrated DNA technologies, San Diego, CA). The plasmids for wild-type and mutant forms of Tra2β(ΔN), SRPK1, SRSF1, and CLK1 were transformed into the BL21 (DE3) *E. coli* strain and grown at 37°C in LB broth supplemented with 100 μg/ml ampicillin. Protein expression was induced with 1 μg/mL IPTG at room temperature for 5 hours for SRSF1 and Tra2β(ΔN) and 12 hours for SRPK1, and 2.5 μg/mL IPTG for 16 hours for CLK1. SRPK1, SRPK1(6M), CLK1 and Tra2β(ΔN/RS) were purified by Ni-resin affinity chromatography using published procedures (21, 26). All SRSF1 and Tra2β(ΔN) constructs containing part or all of the RS domain were refolded and purified using a previously published protocol (13).

Phosphorylation Reactions-Manual Mixing

The phosphorylation of wild-type and mutant forms of Tra2β(ΔN) and SRSF1 by SRPK1 and CLK1 were carried out in the presence of 100 mM Mops (pH 7.4), 10 mM free Mg^{2+}, and 5 mg/mL BSA, at 23 °C according to previously published procedures (13). Progress curves were carried out with 1PM enzyme and 0.2 PM SR protein and 100 μM [γ-^{32}P]ATP (4000–8000 cpm $pmol^{-1}$) unless otherwise stated. Competition reactions were carried out using fixed amounts of Tra2β(ΔC) (500 nM) or Tra2β(ΔN) (1 μM) as substrates and varying concentrations of the competitors (substrate inhibitors). All reactions were carried out in a total reaction volume of 10 μL and then were quenched with 10 PL SDS PAGE loading buffer. Phosphorylated SR protein was separated from unreacted ^{32}P-ATP by loading the quenched reaction on an SDS PAGE gel (10 or 16%) and running at 170V for 1 hour. Protein bands corresponding to phosphorylated SR protein were cut from the dried SDS PAGE gel and quantitated on the ^{32}P channel in liquid scintillant. The total amount of phosphoproduct was then determined by considering the specific activity (cpm/min) of the reaction mixture, and the background retention of ^{32}P-ATP in the absence of enzyme.

LysC Proteolysis & Pull Downs

Tra2β(ΔN) (0.25 μM) was phosphorylated using 1 PM SRPK1 in the presence of 50 μM [γ-^{32}P]ATP (4000–8000 cpm $pmol^{-1}$) for 30 minutes in a total volume of 70 PL. This reaction was then split in half and an equal volume of buffer (50 mM Tris pH 8.5, 2 mM EDTA) with and without 0.35 Pg LysC was added and incubated at 37 °C for 90 minutes.

For pull down assays, portions of these reactions were incubated with and without 30 PL Ni^{++} resin at room temperature for 60 minutes on a bench top rotator. The incubated reactions containing Ni^{++} resin were then washed 6 times with 500 PL buffer (25 mM Tris pH 8.5, 0.5% Triton-X 100, 1M NaCl, 15% Glycrol). SDS-PAGE loading buffer was added to the samples which were then boiled for 5 min to release the protein fragments bound to the Ni^{++} resin before spinning down for 5 minutes at 12,000 rpm. Phosphorylated SR protein fragments were visualized using a 20% SDS-PAGE gel run at 170V for 1 hour.

Mass Spectrometric Analyses

MALDI-TOF analyses were carried out using a Voyager DE-STR spectrometer. Tra2β(ΔN) (1 μM) was incubated with SRPK1 (300 nM) and 0.3 mM ATP in the presence of 50mM Mops (pH 7.4) and 10 mM free Mg^{2+} for 1 hr in a total volume of 100 μL at room temperature. Reactions then were quenched with 5% acetic acid, desalted with Zip-tip C_4 and eluted with 80% acetonitrile, 2% acetic acid for MALDI-TOF analysis. Unphosphorylated sample controls were prepared in the same manner, without ATP. The matrix solution consisted of sinapinic in 70% methanol and 0.05% TFA. Final pH of the matrix solution was 2.0.

Rapid Quench Flow Experiments

Pre-steady-state and single turnover kinetic measurements were performed using a KinTek Corp. Model RGF-3 quench flow apparatus following a previously published procedure (17). The apparatus consists of three syringes driven by a stepping motor. Typical experiments were performed by mixing equal volumes of the SRPK1-Tra2β(ΔN) complex in one reaction loop and ^{32}P-ATP (5000–15000 cpm/pmol) in the second reaction loop in the presence of 100 mM Mops (pH 7.4), 10 mM free Mg^{2+}, 5 mg/mL BSA. The reaction was quenched with 30% acetic acid in the third syringe. Phosphorylated Tra2β(ΔN) was separated from unreacted ATP using a filter-binding assay where a portion of each quenched reaction (50 μL) was spotted onto a phosphocellulose filter disk and was washed 3 times with 0.5% phosphoric acid. The filter disks were rinsed with acetone, dried, and counted on the ^{32}P channel in liquid scintillant. The total amount of phosphoproduct was then determined by considering the specific activity (cpm/min) of the reaction mixture, and the background retention of ^{32}P ATP in the absence of enzyme. Retention of the phosphorylated product on the filters was assessed by running quenched reaction samples on SDS-PAGE and counting the bands. Control experiments lacking the Tra2β(ΔN)-SRPK1 complex were run to define a background correction.

Viscosity Studies

The steady-state phosphorylation of Tra2β(ΔN) was monitored using the filter binding assay as described above in the presence of 0–30% sucrose. The relative solvent viscosity (η^{rel}) of the buffer (100 mM Mops, pH 7.4) containing 0–30% sucrose was measured using an Ostwald viscometer and a previously published protocol (27). A η^{rel} of 1.44, 1.83, 2.32, and 3.43, were measured for buffer containing 10, 20, 25, and 30% sucrose at 23 °C.

Data Analysis

In single turnover experiments, the time-dependent production of phosphoproduct was fit to either single or double exponential functions. In pre-steady-state kinetic experiments, the reaction product normalized to the enzyme concentration ([P]/[E]) were fit to equation (1):

$$\frac{[P]}{[E]} = \alpha\,(1 - \exp(-k_b t)) + k_L t \quad (1)$$

where α, k_b, and k_L are the amplitude of the 'burst' phase, the rate constant for the 'burst' phase and the rate constant for the linear phase, respectively. The initial velocity data were fit to the Michaelis-Menten equation to obtain K_m and V_{max}. The V_{max} values were converted to k_{cat} using the total enzyme concentration determined from a Bradford assay ($k_{cat} = V_{max}/E_{tot}$). The rate constants for several steps in the mechanism were extracted from viscosity dependences on several steady-state kinetic parameters according to equations (2–5):

$$k_4 = \frac{k_{cat}}{(k_{cat})^{\eta}} \quad (2)$$

$$k_3 = \frac{k_{cat}}{[1 - (k_{cat})^{\eta}]} \quad (3)$$

$$k_{on}^{ATP} = \frac{k_{cat}/K_{ATP}}{(k_{cat}/K_{ATP})^{\eta}} \quad (4)$$

$$k_{off}^{ATP} = \frac{k_{cat}}{(k_{cat}/K_{ATP})^{\eta}} \times \frac{1 - (k_{cat}/K_{ATP})^{\eta}}{1 - (k_{cat})^{\eta}} \quad (5)$$

where $(k_{cat})^{\eta}$ and $(k_{cat}/K_{ATP})^{\eta}$ are the slopes of plots of the relative steady-state kinetic parameter versus η^{rel}. The dissociation constant (K_I) for a protein construct to SRPK1 was measured using equation (6):

$$\frac{v}{v_o} = \frac{[S] + K_{SR}}{[S] + K_{SR}\left(1 + \frac{[I]}{K_I}\right)} \quad (6)$$

where v_i/v_o is the relative initial velocity (ratio of v in the presence and absence of inhibitor) and [I] is the total substrate inhibitor concentration.

Results

SRPK1 Phosphorylates the RS domain in Tra2β(ΔN)

Since SRPK1 has been shown to phosphorylate exclusively the RS domain of SRSF1 (14) (Fig.1A), we wondered whether other SR proteins show similar regiospecificity. To address this question, we expressed and purified a natural splice variant of the SR protein Tra2β1 that lacks the N-terminal RS domain. This form, named Tra2β(ΔN) throughout, retains the traditional structure of an SR protein with an RRM followed by a C-terminal RS domain (Fig.1A). Although Tra2β(ΔN) contains 8 serines flanking arginines in its RS domain, the single RRM also contains potential SRPK1 sites ($SRRSR_{160}$; Fig. 1B). To identify whether SRPK1 targets the latter serines, we performed a footprinting experiment. Tra2β(ΔN) contains 4 lysines in the RRM (none in the RS domain) that may be cleaved by the protease LysC (Fig. 1B). While Lys-141 lies on the N-terminal side of the potential SRPK1 sites, the remaining lysines (Lys-174,-177,-198) lie on the C-terminal side and their cleavage can be used to map phosphorylation in the putative SRPK1 sequence. Upon phosphorylation and LysC cleavage, Tra2β(ΔN), which typically migrates as a 24 kDa protein on SDS-PAGE, reduces to a 16 kDa polypeptide (Fig. 1C). The radioactivity in this fragment and the remaining substrate account for most (95%) of the total indicating that LysC generates only one major phosphorylated fragment from Tra2β(ΔN). Also, we observed no small bands on

the autoradiogram consistent with a fragment spanning the putative SRPK1 site in the RRM. Pull-down experiments verify that the 16 kDa fragment contains the original C-terminal His tag (Fig. 1B) and likely reflects cleavage at Lys-174 or Lys-177 rather than Lys-141 which is expected to produce a 19 kDa polypeptide. Since Lys-174/177 are C-terminal to the putative phosphorylation segment, SRPK1 is unlikely to phosphorylate within $SRRSR_{160}$. To confirm these results we expressed the RRM of Tra2β(ΔN) and found that it was not phosphorylated by SRPK1 (data not shown). These results indicate that SRPK1 specifically phosphorylates the C-terminal RS domain in Tra2β(ΔN).

Identification of Phosphorylation Sites in the RS domain

To identify which of the serines in the Tra2β(ΔN) RS domain is modified by SRPK1, we initially performed kinetic experiments to measure total phosphoryl content. Although the RS domain contains 8 serines flanking arginines, approximately 5 of those serines are modified by SRPK1 within the time frame of the assay (Fig.1D). This total phosphoryl content obtained from the autoradiogram was verified using MALDI-TOF mass spectrometry (Fig. 1E). To address whether the final Arg-Ser repeat in the RS domain [$(RS)_4$] corresponds to the major sites, we expressed and purified a serine-to-alanine mutant that removes these four serines [Tra2β(ΔN-4RA)] and showed that it is poorly phosphorylated by SRPK1 (Fig.1A,F). The reduction in observed phosphoryl content (5→1) suggests that SRPK1 mainly targets the final $(RS)_4$ region and may also modify one additional, isolated Arg-Ser dipeptide. To determine which serines are modified, we designed a deletion mutant that removes $(RS)_4$ and one additional nearby serine. Tra2β(ΔN/RS2) is not a substrate for SRPK1 (Fig. 1F) indicating that the Ser directly N-terminal to $(RS)_4$ is phosphorylated along with $(RS)_4$. Furthermore, the inability to phosphorylate Tra2β(ΔN/RS2) supports the observation that SRPK1 does not phosphorylate within the RRM. To address whether the C-terminal half of the RS domain is a major site for other splicing kinases, we investigated the phosphorylation of Tra2β(ΔN) by CLK1 which phosphorylates both Arg-Ser and Ser-Pro dipeptides in SR proteins (21). We found that CLK1 modifies about 3 additional serines in Tra2β(ΔN) compared to SRPK1 which likely corresponds to the three Ser-Pro dipeptides in the RS domain (Fig.1 A,G). CLK1 modifies only 2–3 serines in Tra2β(ΔN-4RA) suggesting that CLK1 is targeting the same Arg-Ser repeat as SRPK1. This is further supported by the observation that Tra2β(ΔN/RS2) is very weakly phosphorylated by CLK1 (Fig. 1G). Overall, the data are consistent with a common region of phosphorylation corresponding to the $(RS)_4$ repeat and an isolated dipeptide in the C-terminus of the Tra2β(ΔN) RS domain

Phosphoryl Transfer Step Does not Limit Tra2β(ΔN) Turnover

The phosphoryl transfer step in SRPK1 is very fast and does not limit turnover of the SR protein SRSF1 (17). Since this substrate contains a long Arg-Ser repeat that may facilitate correct alignment of the RS domain and rapid turnover (Fig.1A), we wondered whether the corresponding RS domain in Tra2β(ΔN) which lacks a lengthy repeat segment would be efficiently modified in the active site of SRPK1. In steady-state progress curves with equal amounts of enzyme and saturating substrate, Tra2β(ΔN) is turned over by SRPK1 at a much slower rate than SRSF1 (Fig. 2A). These differences correspond to decreases in k_{cat} from 1 sec^{-1} for SRSF1 to 0.03 sec^{-1} for Tra2β(ΔN) (Fig 1A; inset). To determine whether the reduced turnover number for Tra2β(ΔN) is the result of an impaired phosphoryl transfer step, we performed rapid quench flow experiments to isolate the first phosphorylation event. In single turnover experiments, we showed that Tra2β(ΔN) phosphorylation occurs in two discrete kinetic phases (Fig.2B). The initial phase (0.2 sec^{-1}) includes the first phosphorylation event and is about 7-fold faster than k_{cat}, suggesting that the phosphoryl transfer step is fast relative to turnover. Interestingly, while k_{cat} reflects mostly early phosphorylation events, the initial velocity of the second phase in the single turnover

experiment (0.02 sites/sec) is close to k_{cat} suggesting that a common rate-limiting step may control multisite phosphorylation in Tra2β(ΔN). To confirm that the phosphoryl transfer step is fast, we performed pre-steady-state kinetic experiments and found that the kinetic profile is consistent with a rapid phosphoryl transfer step or 'burst' phase preceding the linear, steady-state phase (Fig. 2C). The data were fit to equation (1) to obtain a 'burst' rate constant (k_b) of 0.2 sec^{-1}, a value identical to that observed in the first phase of the single turnover experiment. Also, the linear rate constant (k_L = 0.027 sec^{-1}) is close in value to k_{cat} indicating that the experiment also captures the steady-state phase detected at low enzyme concentration. Overall, these data suggest that the phosphoryl transfer step is fast for SRPK1 and does not limit net turnover of Tra2β(ΔN).

A Viscosity-Dependent Step Regulates Tra2β(ΔN) Phosphorylation

Since the phosphoryl transfer step to Tra2β(ΔN) is fast, we wished to determine whether the release of a reaction product could limit k_{cat}. To investigate this question we initially performed viscosometric experiments. If the release of one or both of the products [ADP or phospho-Tra2(ΔN)] controls substrate phosphorylation, k_{cat} should decline with increasing solvent viscosity according to the Stokes-Einstein relationship (28, 29). Using a fixed amount of Tra2β(ΔN), we measured the initial velocity as a function of ATP in the presence of varying amounts of sucrose. Relative k_{cat} (the ratio of k_{cat} in the absence and presence of viscosgen) increases as a function of relative viscosity with a slope value [$(k_{cat})^{\eta}$] of 0.9 (Fig.2C). Since this value is close to the theoretical upper limit of 1, release of one or both of the reaction products is likely to limit k_{cat}. In previous studies, we showed that the net release of products (k_4) and the phosphoryl transfer step (k_3) in a protein kinase reaction can be estimated from k_{cat} and $(k_{cat})^{\eta}$ (28, 29) according to equations (2) and (3). Using this approach, values of 0.32 and 0.036 sec^{-1} can be derived for k_3 and k_4. The former value is similar to the phosphoryl transfer rate constant from the rapid quench flow experiments (Fig 2A,B). These data suggest that Tra2β(ΔN) turnover is limited by a viscosity-dependent step that most likely corresponds with product release.

Investigating ADP Release Rate Using $C_{AT}T_{RAP}$ Experiments

Since ADP release limits multisite phosphorylation of SRSF1 by SRPK1 (16, 17), we wished to ask whether a similar product dissociation step could control Tra2β(ΔN) turnover. To accomplish this we employed a catalytic trapping ($C_{AT}T_{RAP}$) experiment (30) in which the SRPK1:Tra2β(ΔN) complex is first pre-incubated with ADP before reaction initiation with excess ATP in the rapid quench flow instrument (Fig.3A). Using this methodology, we found that ADP pre-incubation resulted in a small 'lag' relative to the control lacking ADP before resumption of product formation (Fig. 3B). Two criteria are used to verify that this sigmoidal behavior is not the result of: 1) inadequate, initial complex formation with ADP or 2) inefficient trapping of the ADP-free complex with ATP (28). First, since the total ADP concentration is more than 10-fold above its K_I (17), most of the initial enzyme-substrate complex should be saturated with ADP prior to ATP addition. Also, if some of the complex lacked bound ADP, then a small 'burst' phase would be detected rather than a 'lag' phase but this is not the case. Second, since the linear rates of the reaction with and without ADP are similar (t > 15 sec), sufficient ATP is added to compete with ADP and achieve maximum turnover. These observations establish that SRPK1 initially forms a complex with ADP and that enough ATP is present to trap this complex in the rapid quench experiment.

To analyze the $C_{AT}T_{RAP}$ experiments, the data were simulated using the mechanism in Fig. 3A. The association rate constant for ATP (k_{on}^{ATP}) was determined from the ratio of k_{cat}/K_m for ATP (k_{cat}/K_{ATP}; 2.9 $mM^{-1}sec^{-1}$) and the viscosity sensitivity on this parameter $(k_{cat}/K_{ATP})^{\eta}$ (Fig. 2C) using equation (4) and was set constant for the simulations (7 $mM^{-1}sec^{-1}$).

After fixing k_{on}^{ATP}, we obtained an optimal simulation for the kinetic data with values of 0.23 and 0.028 sec^{-1} for k_3 and k_4 in the absence of ADP. We then simulated the data with ADP pre-equilibration and obtained optimal fitting using a value of 0.34 sec^{-1} for the ADP dissociation rate constant (k_{off}^{ADP}). This rate constant is close to a prior value (1 sec^{-1}) using SRSF1 as a substrate in the $C_{AT}T_{RAP}$ experiment (17). Since k_{off}^{ADP} is about 7-fold larger than k_{cat}, ADP release does not limit net Tra2β(ΔN) phosphorylation. To provide further evidence that nucleotides exchange rapidly in the active site relative to k_{cat}, we calculated the dissociation rate constant for ATP (k_{off}^{ATP}) using k_{cat}, $(k_{cat})^{\eta}$, $(k_{cat}/K_{ATP})^{\eta}$ and equation (5). With this analysis, we can estimate a value of 0.48 sec^{-1} for k_{off}^{ATP} from the enzyme-substrate complex, a value close to k_{off}^{ADP} obtained from the $C_{AT}T_{RAP}$ experiments. In summary, these experiments show that the release of ADP from SRPK1 is larger than k_{cat} and does not control the rate of Tra2β(ΔN) turnover.

Monitoring Tra2β(ΔN) Release Using Start-Trap Experiments

The rapid quench flow experiments show that the phosphoryl transfer and ADP release steps are fast suggesting that phospho-Tra2β(ΔN) dissociation controls overall turnover. To address this we performed a start-trap experiment to evaluate whether protein dissociation occurs during normal catalytic cycling. In this experiment the enzyme-substrate complex is mixed with ATP in the absence and presence of a kinase-inactive form of SRPK1 (kdSRPK1) (14). In prior studies, we showed that a K→M mutation in the active site of SRPK1 generates an inactive kinase that binds tightly to SRSF1 and inhibits its phosphorylation (19). In the start-trap experiment, if any phospho-forms of Tra2β(ΔN) are released from the active site during the reaction, kdSRPK1 will trap them and inhibit further phosphorylation. However, if Tra2β(ΔN) is phosphorylated without dissociation from SRPK1 in a processive manner, then kdSRPK1 will not affect the reaction. To evaluate whether the inactive kinase is an effective trap for Tra2β(ΔN), we pre-incubated kdSRPK1 with the SRPK1:Tra2β(ΔN) complex before the addition of ATP. In this trap-start experiment, kdSRPK1 strongly inhibited Tra2β(ΔN) phosphorylation compared to the control reaction lacking kdSRPK1 (Fig. 3C). Based on the initial portion of the progress curve, the reaction velocity is, at least, 10-fold lower in the presence of kdSRPK1. When kdSRPK1 is added simultaneously with ATP in the start-trap experiment, it also strongly inhibited the progress curve compared to the control reaction lacking kdSRPK1 (Fig. 3C). This result is consistent with a mechanism in which Tra2β(ΔN) is released after each round of phosphorylation in a distributive manner. These findings suggest that phospho-Tra2β(ΔN) dissociation could play a role in controlling net SR protein turnover.

In the start-trap experiment, we observed a small, rapid generation of phospho-Tra2β(ΔN) in the earliest time points equivalent to roughly one site relative to the control reaction (Fig. 3C). This may be the result of slow exchange of Tra2β(ΔN) from the enzyme-substrate complex relative to forward catalysis. To attain additional information on how fast Tra2β(ΔN) exchanges with SRPK1 we measured the dissociation rate constant for the substrate using the viscosity-dependent data in Fig. 2D. Substituting $(k_{cat}/K_{SR})^{\eta}$ for $(k^{cat}/K_{ATP})^{\eta}$ in equation (5), we estimated a k_{off} for Tra2β(ΔN) of 0.06 sec^{-1}, a value close to k_{cat}. This exchange rate for the protein substrate is slower than k_3 and could account for the rapid generation of phospho-product in the initial phase of the start-trap experiment. To further verify that Tra2β(ΔN) dissociates slowly from SRPK1 we measured its affinity in a competition experiment (14). In this method, we measured the phosphorylation velocity of a fixed amount of a truncated form of Tra2β that lacks the C-terminal RS domain but maintains the N-terminal RS domain [Tra2β(ΔC)] as a function of increasing Tra2β(ΔN). The phosphorylation of the alternate substrate Tra2β(ΔC) declines as that for Tra2β(ΔN) increases (Fig. 3D). By fitting the data to a standard equation for competitive inhibition

[equation (6)] we obtained a K_I for Tra2β(ΔN) of 11 nM, a value close to the substrate K_m of 35 nM (Fig. 3D). Using the association rate constant for Tra2β(ΔN) determined from the viscosity-dependent data (1.1 $\mu M^{-1}sec^{-1}$), we can then use the K_I to estimate a value of 0.012 sec^{-1} for k_{off}, a value close to k_{cat}. Overall, the data garnered from rapid quench flow, start-trap, competition and viscosity experiments support a model where the phosphoryl transfer and ADP release steps are fast and protein product dissociation is a necessary step after each round of phosphorylation. This protein release step is slow and is likely to limit the net rate of Tra2β(ΔN) catalysis.

RS Domain Drives High Affinity Binding of Tra2β(ΔN)

To determine what structural factors govern high affinity binding of Tra2β(ΔN), we studied the binding of several truncated forms of this substrate (Fig. 4A) using a competition assay. In this experiment, we monitored the phosphorylation of a fixed amount of Tra2β(ΔN) with increasing Tra2β(ΔN/RRM), an alternate substrate, and two nonphosphorylatable forms of Tra2β(ΔN) [Tra2β(ΔN/RS2) & Tra2β(ΔN/RS)] (Fig. 4B). In general, we discovered that sequences containing the RS domain are important for inhibiting phosphorylation of the control substrate Tra2β(ΔN). By fitting the velocity data to equation (6) we found that the full RS domain [Tra2β(ΔN/RRM)] binds well to SRPK1 with a K_I of 45 nM, a value similar to the substrate K_m and only 4-fold higher than the K_I for Tra2β(ΔN). In comparison, the construct lacking the RS domain [Tra2β(ΔN/RS)] did not inhibit Tra2β(ΔN) phosphorylation (Fig.4A,B) implying that the free RRM does not interact well with SRPK1. These findings suggest that the RS domain mostly drives high affinity binding of Tra2β(ΔN). Since only a portion of the RS domain is phosphorylated by SRPK1, we wished to determine whether either half of the RS domain participates in high affinity interactions by measuring the binding affinity of Tra2β(ΔN/RS2) which deletes the C-terminal portion of the RS domain. We found that Tra2β(ΔN/RS2) could inhibit Tra2β(ΔN) with a K_I of 180 nM, a value 5-fold higher than the substrate K_m and 16-fold higher than the K_I for Tra2β(ΔN). In summary, these findings indicate that RS domain drives high affinity binding of Tra2β(ΔN) to SRPK1. Although the N-terminus provides some stability, the C-terminus of the RS domain is the main driver of high affinity binding of Tra2β(ΔN).

Tra2β(ΔN) Bypasses the Docking Groove in SRPK1 for RS Domain Phosphorylation

Rapid phosphorylation of SRSF1 is dependent on an electronegative docking groove in the large lobe of the kinase domain of SRPK1 that binds N-terminal Arg-Ser repeats prior to translocation into the active site (15) (Fig. 5A). Mutations in this docking groove result in a less efficient kinase that randomly phosphorylates the RS domain of SRSF1 (14). To determine whether this groove plays a role in phosphorylating Tra2β(ΔN) we performed single turnover experiments using a mutant form of SRPK1 in which 6 electronegative residues in the groove are replaced with alanine [SRPK1(6M)] (14). As previously observed, SRSF1 phosphorylation is reduced for SRPK1(6M) owing to a large decrease in the amplitude for the initial phase compared to the wild-type kinase (Fig. 4C). These findings show that fast, multisite phosphorylation of SRSF1 is facilitated by a functioning docking groove in SRPK1. In comparison, Tra2β(ΔN) was phosphorylated at similar rates by SRPK1(6M) and SRPK1 (Fig. 4D). Also, mutation of the docking groove had no impact on the net phosphoryl content of Tra2β(ΔN) in the time frame of the assay. Both SRPK1 and SRPK1(6M) added about 5 phosphates onto Tra2β(ΔN). Overall, these findings suggest that, unlike SRSF1, Tra2β(ΔN) does not require a functioning docking groove in SRPK1 for efficient RS domain phosphorylation.

Discussion

SRPK1 phosphorylates a strand of eleven consecutive serines in the RS domain of SRSF1 using a novel sequential mechanism where the kinase moves in a strict N-terminal direction (13, 31). Phosphorylation initiation is enforced by a conserved, electronegative docking groove in the large lobe of the kinase domain that binds N-terminal dipeptides and positions the C-terminal dipeptides in the active site for the first round of catalysis (Fig. 5A). Arg-Ser dipeptides in the RS domain then move from the docking groove to the active site in a step-wise manner until the entire strand is phosphorylated. Prior studies indicate that about 5–8 serines are phosphorylated without dissociation of the SR protein (13). This processive phase is transitory as the stability of the SRPK1:SRSF1 complex declines with increasing phosphoryl content of the RS domain, thus, facilitating protein dissociation in late stages of the reaction (17). Mutagenesis studies have shown that both directionality and processive phosphorylation is dependent on a functioning docking groove (14). Despite its apparent complexity, the phosphorylation of the RS domain in SRSF1 is highly efficient. The individual catalytic and dipeptide translocation steps are very fast implying that movement of the RS domain does not present a significant barrier. Rather, slow release of ADP (nucleotide exchange) controls multisite phosphorylation of this SR protein (17). While SRSF1 contains a very long Arg-Ser strand that is capable of spanning both the docking groove and active site, many SR proteins contain much shorter repeat regions raising the question of how these substrates are processed by SRPK1.

Adapting to Other RS Domain Configurations

While many SR proteins present a mix of long and short Arg-Ser repeats (eg., SRSF1 & 2), some lack any repeats above 5 or 6 dipeptides (Fig. S1). For example, SRSF4, 6, 7, & 10 contain Arg-Ser repeats of 1–4 dipeptides in length raising the question of how such SR proteins are activated by SRPK1 given the length constraints imposed by the docking groove and active site. Using Tra2β(ΔN) as a substrate, we investigated the consequences of an RS domain with more truncated Arg-Ser segments in light of the phosphorylation model established for SRSF1 (Fig. 5A). Through detailed kinetic analyses, we found that the mechanism of phosphorylation shifts substantially with the nature of the RS domain. While the longer repeat in SRSF1 is phosphorylated using several processive steps that are limited by ADP release, Tra2β(ΔN) is phosphorylated in a distributive manner where protein release appears to control each round of phosphorylation (Fig. 5B). Of critical importance is the observation that conserved elements of the kinase structure are dispensable depending on the RS domain. While the docking groove in SRPK1 is essential for rapid, directional phosphorylation of SRSF1 (14), it appears to be unnecessary for Tra2β(ΔN) phosphorylation (Fig 4D). Such a finding suggests that the N-terminal portion of the RS domain may not reside in the docking groove or its presence has no impact during multiple catalytic cycles (Fig. 5B). These results strongly indicate that the docking groove may be important for the phosphorylation of lengthy Arg-Ser repeats but may be circumvented for shorter Arg-Ser repeats.

Our new kinetic data indicate that changes in the RS domain landscape have profound effects on the phosphorylation mechanism. While RS domain translocation is fast and ADP release slow for SRSF1 phosphorylation, the rate-limiting step for Tra2β(ΔN) phosphorylation is protein release. A critical question is how does SRPK1 process the two RS domains using such different kinetic parameters yet bind the SR proteins with equivalent affinities? The answer to this question lies in how SRPK1 utilizes its docking groove for these two substrates. Previous studies showed that while essential for rapid, processive phosphorylation of SRSF1, the docking groove plays no significant role in controlling overall binding affinity (14). Thus, the groove serves largely a kinetic function and, as such, offers a low energy barrier for transferring Arg-Ser repeats to the active site compared to the

alternative option of successive SRSF1 dissociation steps. On the other hand, for Tra2β(ΔN), which does not use the docking groove, the contacts for high affinity do not provide a low energy pathway for feeding dipeptides into the active site. From these findings, we speculate that for RS domains with short Arg-Ser repeats that cannot occupy the docking groove, the protein substrate may be required to dissociate and re-bind after each round of phosphorylation, a process that is less efficient and leads to low turnover. Furthermore, given the wide diversity of short versus long repeats (Fig. S1), it is worth speculating whether processive phosphorylation could be isolated to SR proteins with long Arg-Ser dipeptide repeats (e.g., SRSF1 & 2) whereas distributive phosphorylation could be the dominant phosphorylation mode in SR proteins with shorter repeats (e.g., SRSF4, 6, 7 & 10).

Attaining High Affinity Binding Through Flexible Binding Contacts

Deletion analyses indicate that the high affinity contacts for Tra2β(ΔN) are mostly localized to the C-terminal half of the RS domain. This contrasts with SRSF1 where high affinity binding lies in the N-terminus of the RS domain (14). An explanation for such a contrasting mode of recognition for these two substrates may be gleaned from a comparison of the RS domains. While both the N- and C-terminal halves of the SRSF1 and Tra2β(ΔN) RS domains are equally arginine-rich, the N-terminal half of the Tra2β(ΔN) RS domain is uniquely rich in negatively charged residues with 7 aspartates (Fig. 1A). These charges may counteract the arginines in this region depriving SRPK1 of enough stable electrostatic contacts for binding the N-terminus of the RS domain. Indeed, these negative charges may explain both the reliance on C-terminal residues for high affinity binding and the inability to phosphorylate the N-terminal serines in the RS domain of Tra2β(ΔN). For SRSF1 which lacks negatively charged residues in its RS domain, all serines flanking arginines are phosphorylated by SRPK1 (14). However, the RS domain in SRSF1 is not typical with regard to charge distribution. It is worth noting that some SR proteins have negatively charged residues (e.g., SRSF4 has 6 aspartates & 21 glutamates) that could limit phosphorylation of one or more discrete Arg-Ser repeats (Fig. S1). The potential to turn off several sites in Tra2β(ΔN) suggests that RS domain phosphorylation could be more complicated than originally thought and that a combination of Arg-Ser position in context of other controlling residues may generate alternative phosphorylation patterns within the larger SR protein family. Finally, while C-terminal residues in the Tra2β(ΔN) RS domain are the main drivers of high affinity, the N-terminal residues provide some stability. Although we don't think that these residues occupy the docking groove, they could bind to other surfaces on SRPK1. This raises the exciting possibility that different RS domains not parsed through the conserved docking groove may interact at other locations outside the active site, thereby uniquely contributing to multisite phosphorylation.

Conclusions

Much of what we know about RS domain phosphorylation stems from studies on what is considered the prototype for the family, SRSF1. The protein kinase SRPK1 uses a conserved docking groove to efficiently phosphorylate the RS domain of this SR protein using a semi-processive, directional mechanism (Fig. 5A). Since most SR proteins contain short Arg-Ser repeats we explored how a change in the RS domain landscape would affect this mechanism. We found that shifting to a shorter repeat had profound affects on kinetic processing. Rather than occupying the docking groove as in the case of SRSF1, the RS domain of Tra2β(ΔN) appears to bypass this conserved structural element (Fig. 5B). The price of phosphorylating this shorter Arg-Ser repeat is a shift in rate-limiting step from slow nucleotide to protein release and a concomitant change from semi-processive to distributive phosphorylation. Any binding in the docking groove with longer repeats greatly increases phosphorylation

efficiency through the feeding mechanism without significantly improving binding affinity. Thus, the role of the docking groove is one of organization rather than stability. These findings raise the possibility that the docking groove might untangle unproductive structure within lengthy Arg-Ser repeats so that they can be efficiently phosphorylated. Prior computational studies suggest that a peptide of 8 Arg-Ser repeats adopts a helical conformation that may be difficult to phosphorylate without the organizing function of a docking groove (32). In contrast, shorter Arg-Ser repeats may be more unstructured and, therefore, may not require the docking groove. Overall, these findings point to a highly flexible kinase that can readily adopt to a changing RS domain architecture.

Supplementary Material

Refer to Web version on PubMed Central for supplementary material.

Abbreviations

$C_{AT}T_{RAP}$	catalytic trapping
CLK1	Cdc2-like kinase 1
RRM	RNA recognition motif
RS domain	domain rich in arginine-serine repeats
SR protein	splicing factor containing arginine-serine repeats
SRPK1	SR-specific protein kinase 1
SRSF1	SR protein splicing factor 1 (aka ASF/SF2)
Tra2β	transformer 2β protein

References

1. Jurica MS, Moore MJ. Pre-mRNA splicing: awash in a sea of proteins. Molecular cell. 2003; 12:5–14. [PubMed: 12887888]
2. Xiao SH, Manley JL. Phosphorylation of the ASF/SF2 RS domain affects both protein-protein and protein-RNA interactions and is necessary for splicing. Genes & development. 1997; 11:334–344. [PubMed: 9030686]
3. Graveley BR, Hertel KJ, Maniatis T. The role of U2AF35 and U2AF65 in enhancer-dependent splicing. RNA. 2001; 7:806–818. [PubMed: 11421359]
4. Yeakley JM, Tronchere H, Olesen J, Dyck JA, Wang HY, Fu XD. Phosphorylation regulates in vivo interaction and molecular targeting of serine/arginine-rich pre-mRNA splicing factors. J Cell Biol. 1999; 145:447–455. [PubMed: 10225947]
5. Lai MC, Lin RI, Huang SY, Tsai CW, Tarn WY. A human importin-beta family protein, transportin-SR2, interacts with the phosphorylated RS domain of SR proteins. The Journal of biological chemistry. 2000; 275:7950–7957. [PubMed: 10713112]
6. Ngo JC, Chakrabarti S, Ding JH, Velazquez-Dones A, Nolen B, Aubol BE, Adams JA, Fu XD, Ghosh G. Interplay between SRPK and Clk/Sty kinases in phosphorylation of the splicing factor ASF/SF2 is regulated by a docking motif in ASF/SF2. Molecular cell. 2005; 20:77–89. [PubMed: 16209947]
7. Zhou Z, Qiu J, Liu W, Zhou Y, Plocinik RM, Li H, Hu Q, Ghosh G, Adams JA, Rosenfeld MG, Fu XD. The Akt-SRPK-SR axis constitutes a major pathway in transducing EGF signaling to regulate alternative splicing in the nucleus. Molecular cell. 2012; 47:422–433. [PubMed: 22727668]
8. Chalfant CE, Rathman K, Pinkerman RL, Wood RE, Obeid LM, Ogretmen B, Hannun YA. De novo ceramide regulates the alternative splicing of caspase 9 and Bcl-x in A549 lung adenocarcinoma cells. Dependence on protein phosphatase-1. The Journal of biological chemistry. 2002; 277:12587–12595. [PubMed: 11801602]

9. Kohtz JD, Jamison SF, Will CL, Zuo P, Luhrmann R, Garcia-Blanco MA, Manley JL. Protein-protein interactions and 5'-splice-site recognition in mammalian mRNA precursors. Nature. 1994; 368:119–124. [PubMed: 8139654]
10. Wu JY, Maniatis T. Specific interactions between proteins implicated in splice site selection and regulated alternative splicing. Cell. 1993; 75:1061–1070. [PubMed: 8261509]
11. Valcarcel J, Gaur RK, Singh R, Green MR. Interaction of U2AF65 RS region with pre-mRNA branch point and promotion of base pairing with U2 snRNA [corrected]. Science. 1996; 273:1706–1709. [PubMed: 8781232]
12. Cho S, Hoang A, Sinha R, Zhong XY, Fu XD, Krainer AR, Ghosh G. Interaction between the RNA binding domains of Ser-Arg splicing factor 1 and U1-70K snRNP protein determines early spliceosome assembly. Proceedings of the National Academy of Sciences of the United States of America. 2011; 108:8233–8238. [PubMed: 21536904]
13. Ma CT, Velazquez-Dones A, Hagopian JC, Ghosh G, Fu XD, Adams JA. Ordered multi-site phosphorylation of the splicing factor ASF/SF2 by SRPK1. Journal of molecular biology. 2008; 376:55–68. [PubMed: 18155240]
14. Hagopian JC, Ma CT, Meade BR, Albuquerque CP, Ngo JC, Ghosh G, Jennings PA, Fu XD, Adams JA. Adaptable molecular interactions guide phosphorylation of the SR protein ASF/SF2 by SRPK1. Journal of molecular biology. 2008; 382:894–909. [PubMed: 18687337]
15. Ngo JC, Giang K, Chakrabarti S, Ma CT, Huynh N, Hagopian JC, Dorrestein PC, Fu XD, Adams JA, Ghosh G. A sliding docking interaction is essential for sequential and processive phosphorylation of an SR protein by SRPK1. Molecular cell. 2008; 29:563–576. [PubMed: 18342604]
16. Aubol BE, Plocinik RM, McGlone ML, Adams JA. Nucleotide release sequences in the protein kinase SRPK1 accelerate substrate phosphorylation. Biochemistry. 2012; 51:6584–6594. [PubMed: 22839969]
17. Aubol BE, Adams JA. Applying the brakes to multisite SR protein phosphorylation: substrate-induced effects on the splicing kinase SRPK1. Biochemistry. 2011; 50:6888–6900. [PubMed: 21728354]
18. Colwill K, Feng LL, Yeakley JM, Gish GD, Caceres JF, Pawson T, Fu XD. SRPK1 and Clk/Sty protein kinases show distinct substrate specificities for serine/arginine-rich splicing factors. The Journal of biological chemistry. 1996; 271:24569–24575. [PubMed: 8798720]
19. Velazquez-Dones A, Hagopian JC, Ma CT, Zhong XY, Zhou H, Ghosh G, Fu XD, Adams JA. Mass spectrometric and kinetic analysis of ASF/SF2 phosphorylation by SRPK1 and Clk/Sty. The Journal of biological chemistry. 2005; 280:41761–41768. [PubMed: 16223727]
20. Ma CT, Ghosh G, Fu XD, Adams JA. Mechanism of dephosphorylation of the SR protein ASF/SF2 by protein phosphatase 1. Journal of molecular biology. 2010; 403:386–404. [PubMed: 20826166]
21. Aubol BE, Plocinik RM, Hagopian JC, Ma CT, McGlone ML, Bandyopadhyay R, Fu XD, Adams JA. Partitioning RS Domain Phosphorylation in an SR Protein through the CLK and SRPK Protein Kinases. Journal of molecular biology. 2013
22. Hofmann Y, Lorson CL, Stamm S, Androphy EJ, Wirth B. Htra2-beta 1 stimulates an exonic splicing enhancer and can restore full-length SMN expression to survival motor neuron 2 (SMN2). Proceedings of the National Academy of Sciences of the United States of America. 2000; 97:9618–9623. [PubMed: 10931943]
23. Glatz DC, Rujescu D, Tang Y, Berendt FJ, Hartmann AM, Faltraco F, Rosenberg C, Hulette C, Jellinger K, Hampel H, Riederer P, Moller HJ, Andreadis A, Henkel K, Stamm S. The alternative splicing of tau exon 10 and its regulatory proteins CLK2 and TRA2-BETA1 changes in sporadic Alzheimer's disease. Journal of neurochemistry. 2006; 96:635–644. [PubMed: 16371011]
24. Stoilov P, Daoud R, Nayler O, Stamm S. Human tra2-beta1 autoregulates its protein concentration by influencing alternative splicing of its pre-mRNA. Human molecular genetics. 2004; 13:509–524. [PubMed: 14709600]
25. Nayler O, Cap C, Stamm S. Human transformer-2-beta gene (SFRS10): complete nucleotide sequence, chromosomal localization, and generation of a tissue-specific isoform. Genomics. 1998; 53:191–202. [PubMed: 9790768]

26. Aubol BE, Chakrabarti S, Ngo J, Shaffer J, Nolen B, Fu XD, Ghosh G, Adams JA. Processive phosphorylation of alternative splicing factor/splicing factor 2. Proceedings of the National Academy of Sciences of the United States of America. 2003; 100:12601–12606. [PubMed: 14555757]
27. Grant BD, Adams JA. Pre-steady-state kinetic analysis of cAMP-dependent protein kinase using rapid quench flow techniques. Biochemistry. 1996; 35:2022–2029. [PubMed: 8639687]
28. Adams JA, Taylor SS. Energetic limits of phosphotransfer in the catalytic subunit of cAMP-dependent protein kinase as measured by viscosity experiments. Biochemistry. 1992; 31:8516–8522. [PubMed: 1390637]
29. Wang C, Lee TR, Lawrence DS, Adams JA. Rate-determining steps for tyrosine phosphorylation by the kinase domain of v-fps. Biochemistry. 1996; 35:1533–1539. [PubMed: 8634284]
30. Zhou J, Adams JA. Participation of ADP dissociation in the rate-determining step in cAMP-dependent protein kinase. Biochemistry. 1997; 36:15733–15738. [PubMed: 9398302]
31. Ma CT, Hagopian JC, Ghosh G, Fu XD, Adams JA. Regiospecific phosphorylation control of the SR protein ASF/SF2 by SRPK1. Journal of molecular biology. 2009; 390:618–634. [PubMed: 19477182]
32. Hamelberg D, Shen T, McCammon JA. A proposed signaling motif for nuclear import in mRNA processing via the formation of arginine claw. Proceedings of the National Academy of Sciences of the United States of America. 2007; 104:14947–14951. [PubMed: 17823247]
33. Kuzmic P. Program DYNAFIT for the analysis of enzyme kinetic data: application to HIV proteinase. Anal Biochem. 1996; 237:260–273. [PubMed: 8660575]

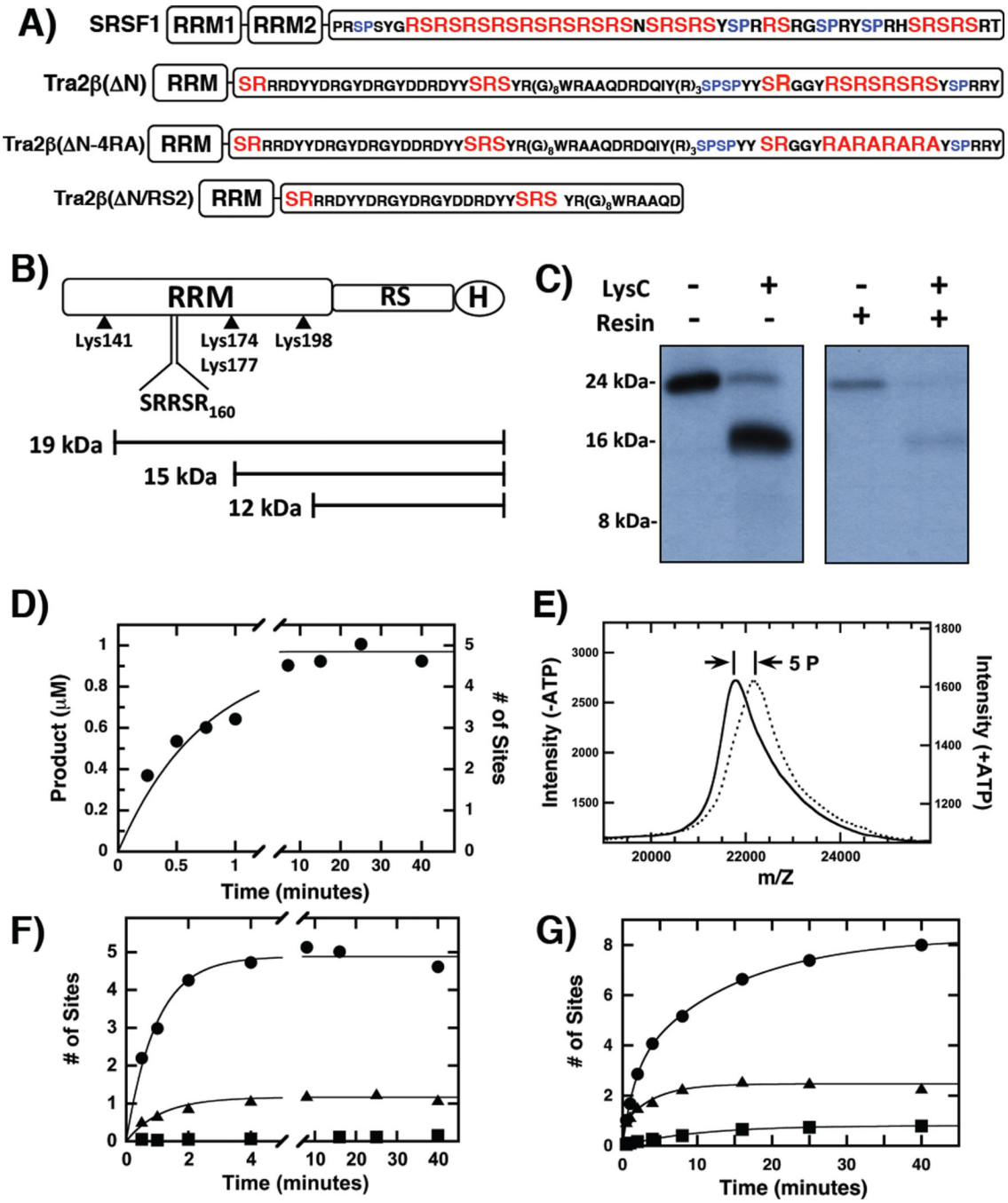

Figure 1. Mapping phosphorylation sites in Tra2β(ΔN)

A) C-terminal RS domain sequences in SRSF1, Tra2β(ΔN), Tra2β(ΔN-4RA) & Tra2β(ΔN/RS2). Ser-Pro and Arg-Ser dipeptides are colored red and blue. B) Lysines in Tra2β(ΔN). Expected LysC fragment sizes containing the C-terminal His tag (H). C) LysC cleavage of Tra2β(ΔN). Substrate is phosphorylated using SRPK1 and ^{32}P-ATP and proteolyzed with LysC. The products are bound to the Ni-resin and washed. D) Progress curve for the phosphorylation of Tra2β(ΔN) (0.2 μM) by SRPK1 (1 μM). The data are fit to a single exponential function with an amplitude of 0.97 ± 0.04 μM (4.8 sites) and a rate constant of 1.4 ± 0.16 min^{-1}. E) MALDI-TOF for Tra2β(ΔN). Major peak at 21.7 kDa for unphosphorylated Tra2β(ΔN) (solid line) increases to 22.1 kDa in the presence of ATP

(dotted line) consistent with the addition of 5 phosphates. F) Progress curves for the phosphorylation of Tra2β(ΔN) (●), Tra2β(ΔN-4RA) (▲) and Tra2β(ΔN/RS2) (■) by SRPK1. The data were fit to amplitudes of 4.9 ± 0.1 and 1.2 ± 0.05 sites and rate constants of 1 ± 0.1 and 0.9 ± 0.14 min^{-1} for Tra2β(ΔN) and Tra2β(ΔN-4RA). G) Progress curves for the phosphorylation of Tra2β(ΔN) (●), Tra2β(ΔN-4RA) (▲) and Tra2β(ΔN/RS2) (■) by CLK1. The data were fit to a double exponential function with amplitudes of 2.9 ± 0.26 and 5.4 ± 0.19 sites and rate constants of 0.65 ± 0.07 and 0.07 ± 0.007 min^{-1} for Tra2β(ΔN) and amplitudes of 0.8 ± 0.23 and 1.7 ± 0.07 sites and rate constants of 5.9 ± 3 and 0.25 ± 0.07 min^{-1} for Tra2β(ΔN-4RA). The data for Tra2β(ΔN/RS2) were fit to a single exponential function with an amplitude and rate constant of 0.8 ± .02 sites and 0.10 ± .01 min^{-1}.

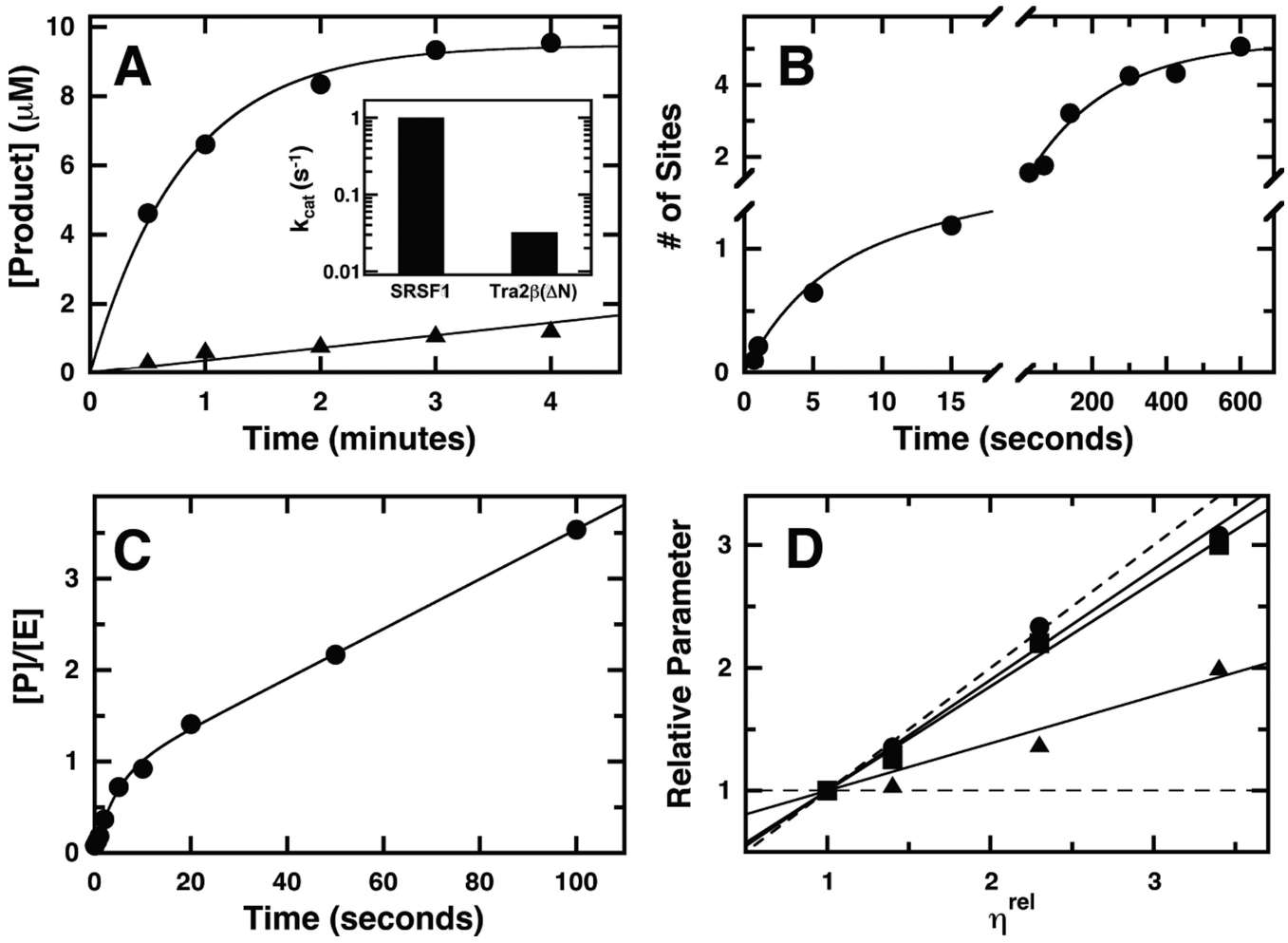

Figure 2. Measuring the phosphoryl transfer step to Tra2β(ΔN)

A) Steady-state progress curves. SRPK1 (200 nM) is mixed with 1 μM SRSF1 (●) and Tra2β(ΔN) (▲). For SRSF1, the data are fit to a single exponential function with an amplitude and rate constant of 9.5 ± 0.2 μM and 1.2 ± 0.10 min^{-1}. For Tra2β(ΔN), the data are fit to a linear function with a slope of 0.36 ± 0.04 μM/min. Inset shows a comparison of k_{cat} obtained from plots of initial velocity versus both substrates. B) Single turnover analyses. SRPK1 (2 μM) and Tra2β(ΔN) (0.1 μM) are mixed with ATP (100 μM) in the rapid quench flow machine and the data are fit to a double exponential function with amplitudes of 0.9 ± 0.2 and 4.3 ± 0.3 sites and rate constants of 0.21 ± 0.10 and 0.005 ± 0.001 sec^{-1}. C) Pre-steady-state kinetic analyses. SRPK1 (0.25 μM) and Tra2β(ΔN) (1 μM) are mixed with ATP (100 μM) in the rapid quench flow machine and the data are fit to equation (1) to obtain values of 0.82 ± 0.08, 0.23 ± 0.04 sec^{-1}, and 0.027 ± 0.008 sec^{-1} for α, k_b, and k_L, respectively. D) Viscosity effects on k_{cat} (●), k_{cat}/K_{SR} (■), and k_{cat}/K_{ATP} (▲). Parameters are displayed as a ratio in the absence and presence of varying sucrose concentrations against the relative buffer viscosity (η^{rel}). The slopes for k_{cat} [$(k_{cat})^{\eta}$], k_{cat}/K_{SR} [$(k_{cat}/K_{SR})^{\eta}$], and k_{cat}/K_{ATP} [$(k_{cat}/K_{ATP})^{\eta}$] are 0.90 ± 0.04, 0.85 ± 0.03, and 0.40 ± 0.04, respectively. In the absence of viscosogens, values of 0.032 ± 0.003 sec^{-1}, 0.91 ± 0.20 $\mu M^{-1}sec^{-1}$, 2.9 ± 0.5 $mM^{-1}sec^{-1}$ were obtained for k_{cat}, k_{cat}/K_{SR}, and k_{cat}/K_{ATP}, respectively. The dotted lines represent theoretical slope values of 0 and 1.

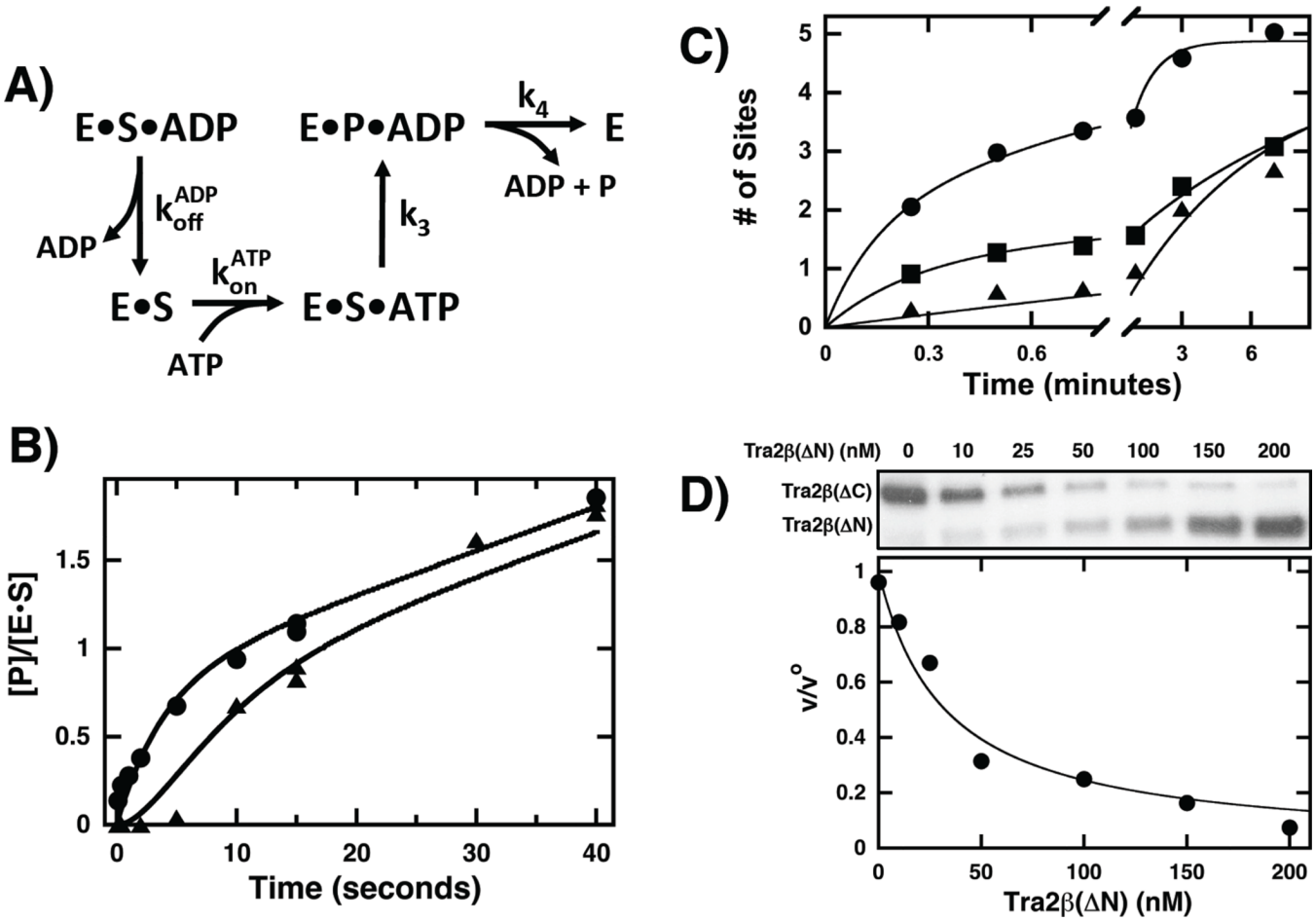

Figure 3. Analysis of product release for Tra2β(ΔN) turnover

A) Mechanism used to analyze kinetic data experiment. S=Tra2β(ΔN); P=phospho-Tra2β(ΔN); E=SRPK1. B) $C_{AT}T_{RAP}$ experiment. SRPK1 is pre-incubated with Tra2β(ΔN) in the absence (●) and presence (▲) of 120 μM ADP in one syringe (60 μM in reaction) and then mixed with ATP (600 μM in reaction) to start the reaction. The data are simulated using DynaFit (33) and the mechanism in Fig.3A to obtain values of 0.34 sec^{-1}, 0.23 sec^{-1}, and 0.024 sec^{-1} for k_{off}, k_3, and k_4, respectively. A value of 7 $mM^{-1}sec^{-1}$ for the ATP k_{on} was used for both simulations. C) Start-Trap experiment. A complex of SRPK1 (1 μM) and Tra2β(ΔN) (0.2 μM) is mixed with ATP (60 μM) in the absence (●) and presence (■) of kdSRPK1 (60 μM). In a control experiment (trap-start), the complex is pre-equilibrated with kdSRPK1 before reaction initiation with ATP (▲). The reaction in the absence of kdSRPK1 is fit to a double exponential function with amplitudes of 1.40 ± 0.14 and 3.40 ± 0.13 sites and rate constants of 9 ± 5 and 1 ± 0.15 min^{-1}, respectively. The start-trap data are fit to a double exponential function with amplitudes of 1.3 ± 0.15 and 3.7 ± 0.20 sites and rate constants of 3.7 ± 1.2 and 0.10 ± 0.01 min^{-1}, respectively. The trap-start data are fit to a single exponential function with an amplitude of 4.5 ± 0.5 sites and a rate constant of 0.15 ± 0.02 min^{-1}. D) Competition experiment. SRPK1 (5 nM), Tra2β(ΔC) (500 nM), ATP (60 μM) and varying amounts of Tra2β(ΔN) (0–200 nM) are allowed to react for 2.5 minutes. The relative velocity for Tra2β(ΔC) obtained from the autoradiogram is plotted as a function of Tra2β(ΔN) and fitted to equation (6) to obtain a K_I of 11 ± 2 nM for Tra2β(ΔN) using a K_m of 270 nM for Tra2β(ΔC) measured in separate experiments.

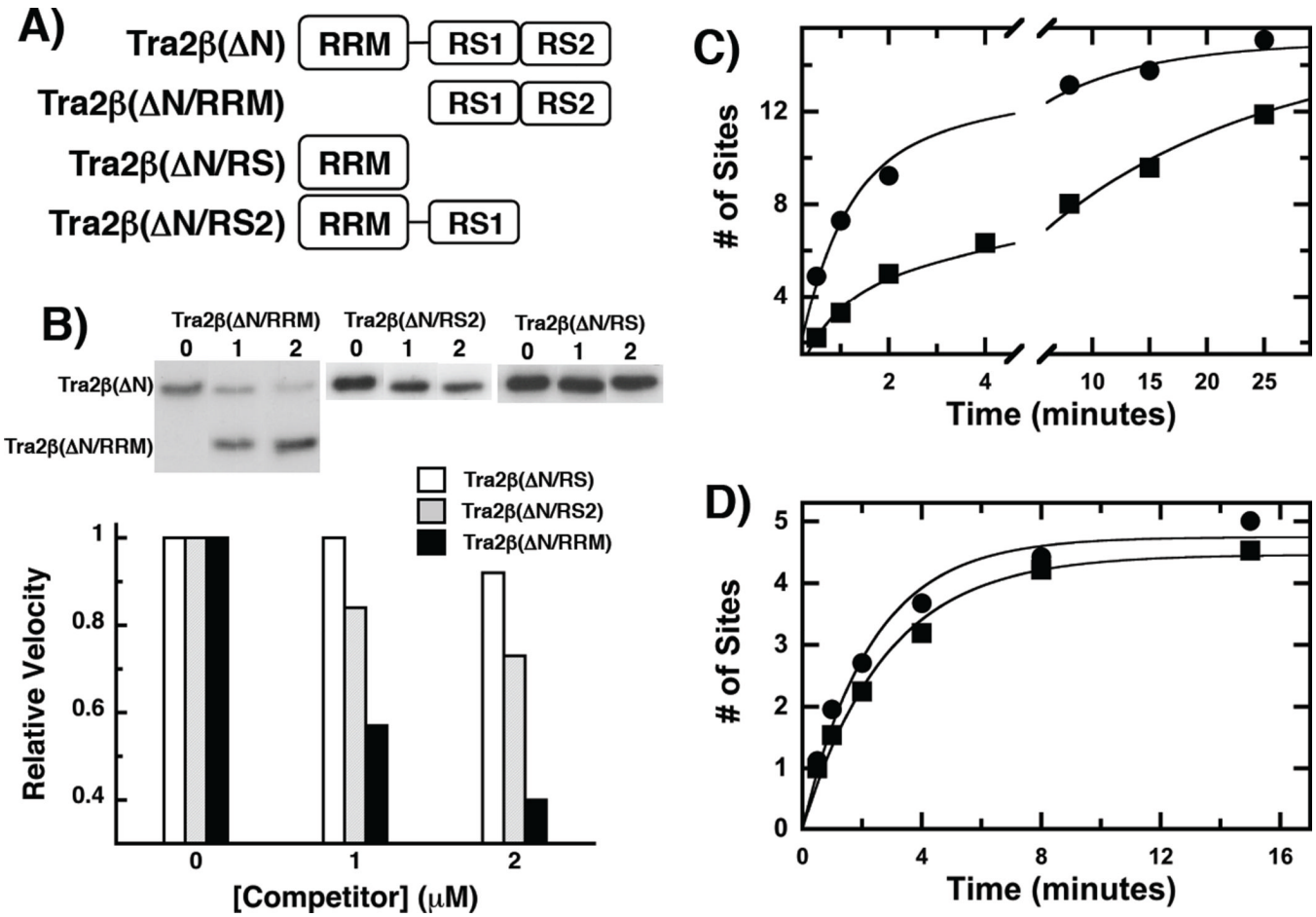

Figure 4. Polypeptide segments important for SRPK1-Tra2β(ΔN) interactions

A) Deletion Constructs. B) Binding of Tra2β(ΔN) deletions. Relative initial velocities for Tra2β(ΔN) (1 μM) phosphorylation are obtained from the autoradiogram and displayed as a function of 1 or 2 μM of the following competitors: Tra2β(ΔN/RS), Tra2β(ΔN/RRM), and Tra2β(ΔN/RS2). C) Progress curves for the phosphorylation of SRSF1 by SRPK1 (●) and SRPK1(6M) (■). The data are fit to a double exponential function to obtain amplitudes and rate constants of 10 ± 1 and 5 ± 1 sites and 1.2 ± 0.1 and 0.11 ± .02 min^{-1} for SRPK1 and amplitudes and rate constants of 4 ± 0.5 and 11 ± 0.5 sites and 1.3 ± 0.2 and 0.050 ± 0.022 min^{-1} for SRPK1(6M). D) Progress curves for the phosphorylation of Tra2β(ΔN) by SRPK1 (●) and SRPK1(6M) (■). The data are fit to a single exponential function to obtain an amplitude and rate constant of 4.7 ± 0.2 sites and 0.44 ± 0.06 min^{-1} for SRPK1 and an amplitude and rate constant of 4.5 ± 0.2 sites and 0.36 ± 0.04 min^{-1} for SRPK1(6M).

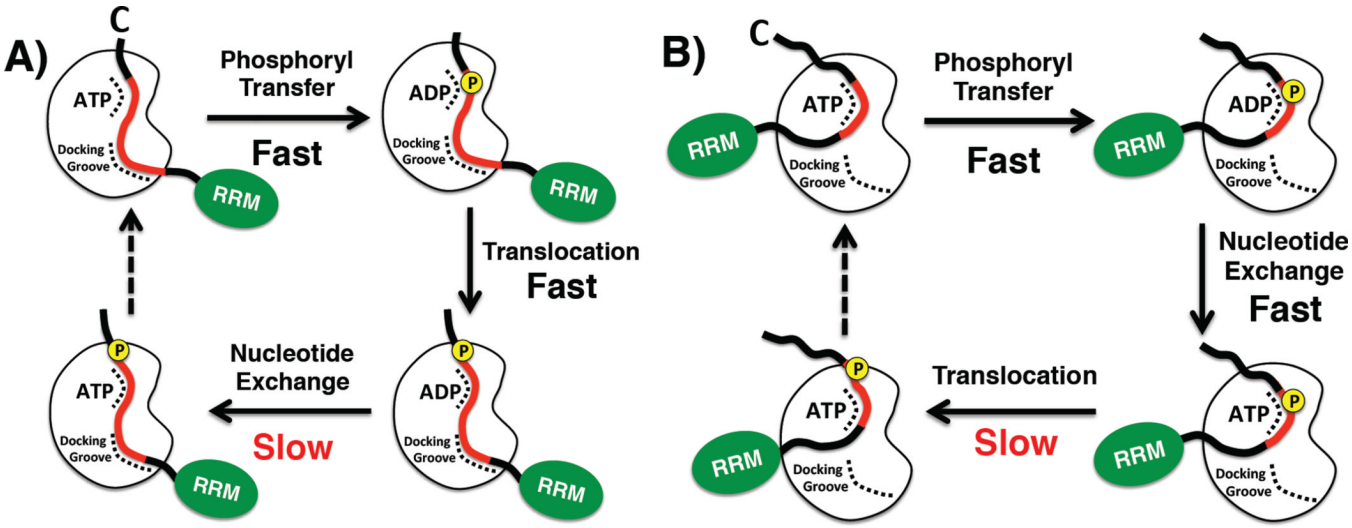

Figure 5. Mechanisms for RS domain phosphorylation

A) Long Arg-Ser repeats. Docking groove orients RS domain for efficient phosphoryl transfer and translocation of N-terminal dipeptides into the active site. The rate-limiting step is ADP release (nucleotide exchange). B) Short Arg-Ser repeats. Docking groove is bypassed and only local residues in the active site control RS domain phosphorylation. Both the phosphoryl transfer and nucleotide exchange steps are fast while the translocation step is slow. The red portions of the RS domains designate Arg-Ser-rich regions